ISSN 1063-7834, Physics of the Solid State, 2018, Vol. 60, No. 1, pp. 23–30. © Pleiades Publishing, Ltd., 2018.
Original Russian Text © A.S. Nogai, S.Yu. Stefanovich, A.A. Bush, D.E. Uskenbaev, A.A. Nogai, 2018, published in Fizika Tverdogo Tela, 2018, Vol. 60, No. 1, pp. 25–32.

SEMICONDUCTORS

Dipole Ordering and Ionic Conductivity in NASICON-Type $Na_3Cr_2(PO_4)_3$ Structures

A. S. Nogai[a,*], S. Yu. Stefanovich[b], A. A. Bush[c], D. E. Uskenbaev[a], and A. A. Nogai[a]

[a] *Kazakh Agrotechnical University, Astana, 010000 Kazakhstan*
[b] *Karpov Scientific and Research Physicochemical Institute, Moscow, 249033 Russia*
[c] *Moscow Technological University (MIREA), Moscow, 119454 Russia*
**e-mail: nogay06@mail.ru*

Received January 25, 2017; in final form, May 10, 2017

Abstract—The aspects of structure, dipole ordering, and ionic conductivity of the $Na_3Cr_2(PO_4)_3$ crystal with the four polymorphic phases (α, α', β, and γ) have been investigated. The features of the α-$Na_3Cr_2(PO_4)_3$ crystal structure and its dipole ordering and relaxation polarization in the low-temperature α and α' phases have been refined. The occurrence of $Na_3Cr_2(PO_4)_3$ dipole ordering in the α and α' phases and high ionic conductivity in the β and γ phases is attributed to the structural changes in the rhombohedral $\{[Me_2(PO_4)_3]^{-3}\}_{3\infty}$ crystal frame upon phase transformations $\alpha \rightarrow \alpha'$, $\alpha' \rightarrow \beta$, and $\beta \rightarrow \gamma$. A model for explaining the dipole ordering and ionic conductivity phenomena in $Na_3Cr_2(PO_4)_3$ is proposed.

DOI: 10.1134/S1063783418010146

1. INTRODUCTION

The bright representatives of the NASICON family are $Na_3Sc_2(PO_4)_3$ and $Na_3Cr_2(PO_4)_3$ with low ionic conductivity in the low-temperature α and α' phases and high ionic conductivity in the high-temperature β and γ phases [1–3]. Substances with the rhombohedral $\{[Me_2(PO_4)_3]^{-3}\}_{3\infty}$ crystal frames have been already widely used as constructive materials for current sources [4].

Further investigations of specific features of the conductive and dielectric properties of $Na_3Cr_2(PO_4)_3$ can open even wider opportunities for application of the NASICON family of substances.

The aim of this study was to establish the correlation between the structural features and manifestations of the dipole ordering and ionic and superionic states in different $Na_3Cr_2(PO_4)_3$ polymorphic modifications (α, α', β, and γ).

2. EXPERIMENTAL

The $Na_3Cr_2(PO_4)_3$ single crystals were grown by spontaneous crystallization from melt (the charge composition is $3Na_2CO_3 + 2Cr_2O_3 + 6NH_4H_2PO_4$) by cooling at a rate of 15.0 K/min.

The phase and structural parameters of single-crystal $Na_3Cr_2(PO_4)_3$ samples were studied by the X-ray powder and Weissenberg methods on a DRON-3 diffractometer and an RGNS-2 X-ray goniometer (CuK_α radiation).

The nonlinear optical properties of the $Na_3Cr_2(PO_4)_3$ crystal were determined by the second optical harmonic generation (SHG) method using neodymium laser radiation.

The conductive and dielectric properties of the samples were studied on a VM-507 impedance meter in the temperature range of 295–573 K at frequencies of 5–500000 Hz. Contacts were formed by deposition of palladium, which is considered to be an ideally blocking electrode, onto the sample surface.

3. RESULTS AND DISCUSSION

3.1. Results of Synthesis and X-Ray Study of the $Na_3Cr_2(PO_4)_3$ Single Crystal

The synthesized $Na_3Cr_2(PO_4)_3$ single crystals were transparent in the visible range, had a green color, exhibited a weak cleavage, and had the form of rectangular prisms 4 × 2 × 2 mm in size.

The X-ray study showed that the crystals have a monoclinic unit cell (sp.gr. $P2_1/n$) with parameters of $a = 21.18(4)$ Å, $b = 8.65(1)$ Å, $c = 30.56(8)$ Å, and $\gamma = 90.5(1)$ Å corresponding to the unit cell parameters of the α-$Na_3Cr_2(PO_4)_3$ phase, which is consistent with the literature data [5]. In addition, the X-ray rocking study showed that the crystals along the **c** axis are characterized by the superstructure of the type $\mathbf{c} = 2\mathbf{c}_0$.

3.2. Results of Ionic Conductivity Investigations and Noncentrosymmetricity Test for the $Na_3Cr_2(PO_4)_3$ Single Crystal

The measurements of the temperature dependence of the $Na_3Cr_2(PO_4)_3$ crystal conductivity and multiple temperature thermocycling in the heating–cooling modes allowed us to establish the exact reproducibility of the measured data.

The measured temperature dependence of ionic conductivity of the $Na_3Cr_2(PO_4)_3$ crystal along the c axis showed that the $\sigma T(T)$ dependence includes four linear portions corresponding to four polymorphic modifications: α, α', β, and γ (Fig. 1).

The temperature dependence of the electric conductivity (Fig. 1) can be described by the ratio

$$\sigma T = A_i \sum_{i=1}^{n} \exp\left(-\frac{\Delta E_i}{kT}\right), \quad (1)$$

where ΔE_i is the activation energy of ionic conductivity of the i phase, k is the Boltzmann constant, T is the absolute temperature, and A_i are the constant coefficients characterizing the phase states.

Having processed the obtained experimental $\sigma(T)$ data (Fig. 1), we determined the parameters of ion transport and temperatures of the phase transitions of sodium chromium phosphate (Table 1).

It can be seen from Table 1 that the low-temperature α and α' phases of the $Na_3Cr_2(PO_4)_3$ crystal are dielectric, since they have low conductivity and high activation energy.

The X-ray data evidence for the superstructural distortions in α-$Na_3Cr_2(PO_4)_3$ and the crystal noncentrosymmetricity test performed using laser radiation allowed us to establish the absence of a SHG signal, which is typical of antiferroelectric structures. The above data confirm that the ionic conductivity of the α-$Na_3Cr_2(PO_4)_3$ phase is very low (4×10^{-8} $(\Omega\ \text{cm})^{-1}$ at 295 K) and the ionic conductivity activation energy is high (0.62 eV); therefore, this phase can be considered as purely dielectric with the antiferroelectric dipole ordering, where there are almost no mobile ions.

It is worth noting that the $\sigma(T)$ plot contains a kink at $T = 348$ K, which is indicative of the presence of temperature phase transition from α-$Na_3Cr_2(PO_4)_3$ to the α' state ($T_{\alpha \to \alpha'} = 348$ K). The ionic conductivity of the α'-$Na_3Cr_2(PO_4)_3$ phase is 7.9×10^{-6} $(\Omega\ \text{cm})^{-1}$ at 370 K and the ionic conductivity activation energy increases to 0.92 eV, which is typical of dielectrics. The conductivity growth at the phase transition α → α' indicates the crystal structure rearrangement. Probably, the structural transformations at the phase transition $T_{\alpha \to \alpha'}$ facilitates partial elimination of the monoclinic distortion of the crystal frame and the growth of the density of mobile sodium ions, which allows their migration over the crystal.

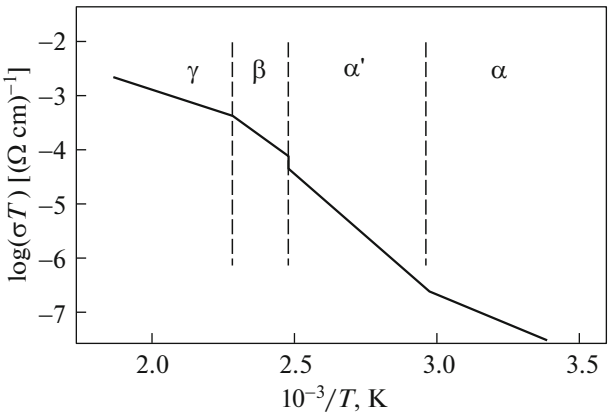

Fig. 1. Temperature dependence of the ionic conductivity for the $Na_3Cr_2(PO_4)_3$ single-crystal sample. Dash-and-dot lines separate the portions corresponding to the α, α', β, and γ phases.

The phase transition from the α' to β phase at a temperature of $T_{\alpha' \to \beta} = 411$ K is accompanied by a small jump of the β-$Na_3Cr_2(PO_4)_3$ crystal conductivity (Fig. 1). At the moment of the phase transition $T_{\alpha' \to \beta}$, the ionic conductivity attains 1.0×10^{-4} $(\Omega\ \text{cm})^{-1}$, which can be attributed to the sharp growth of the density of mobile sodium cations. In this case, the ionic conductivity activation energy slightly decreases (from 0.92 to 0.79 eV), which is indicative of a minor decrease in the potential barrier for cations. A significant increase in the conductivity and a slight decrease in the activation energy at the phase transition α' → β can be attributed to the partial elimination of the monoclinic distortion of the β'-$Na_3Cr_2(PO_4)_3$ crystal frame. Although the ionic conductivity activation

Table 1. Ion transport parameters and phase transformation temperatures for the $Na_3Cr_2(PO_4)_3$ crystal

Phases	Ionic conductivities σ (Ω^{-1} cm^{-1}) at fixed temperatures T	Activation energies ΔE, eV	Phase transformation types	Phase transition temperatures
α	4×10^{-8} ($T = 295$ K)	0.62	α → α'	$T_{\alpha \to \alpha'} = 348$ K
α'	7.9×10^{-6} ($T = 370$ K)	0.92	α' → β	$T_{\alpha' \to \beta} = 411$ K
β	1.0×10^{-4} ($T = 411$ K)	0.79	β → γ	$T_{\beta \to \gamma} = 439$ K
γ	7.5×10^{-4} ($T = 439$ K)	0.39		

energy for β-$Na_3Cr_2(PO_4)_3$ is sufficiently high, a noticeable conductivity jump at the phase transition α' → β allows us to conclude that the conductivity of this phase is close to superionic.

A further increase in temperature leads to the next phase transformation at $T_{\beta\to\gamma}$ = 439 K and, consequently, to even a larger growth of the crystal conductivity (up to 7.5 × 10^{-4} (Ω cm)$^{-1}$ at 439 K) and to a decrease in the ionic conductivity activation energy to 0.39 eV, which can be related to the complete elimination of the monoclinic distortions of the crystal frame as a result of the phase transition β → γ. The γ-$Na_3Cr_2(PO_4)_3$ crystal conductivity can be already considered as superionic.

3.3. Results of Investigations of the Dielectric Properties of the $Na_3Cr_2(PO_4)_3$ Single Crystal

Study of the frequency dependence of the permittivity ε(ω) of the low-temperature α-$Na_3Cr_2(PO_4)_3$ phase shows that the ε value is small and almost frequency-independent (curve *1* in Fig. 2a). These data evidence for a weak effect of the external electric field on the particle polarization processes in this samples. These results can be related to the fact that sodium cations ordered in compensated sodium dipoles were condensed in the bottom of potential wells of the crystal frame (in the bottom of the strained *B* cavities of the crystal frame) due to the monoclinic distortion of the structure (sp. gr. $P2_1/n$), which is quite consistent with the conductivity data and characterizes the α-$Na_3Cr_2(PO)_3$ phase as dielectric (Fig. 2a).

When studying the dielectric properties of α'-$Na_3Cr_2(PO)_3$, we established that this crystal phase is characterized by the polarization relaxation processes, which manifest themselves in the behavior of smoothly decreasing curves *2–5* (Fig. 2a) and the occurrence of relaxation maxima in the frequency dependence of the dissipation factor tanδ(ω) (curves *2–5* in Fig. 2b). Note that with an increase in temperature the smooth ε(ω) curves pass to the sharply decreasing curves (*6–8* in Fig. 2a). As the frequency increases, the relaxation maxima in the tanδ(ω) dependence tend to shift toward higher frequencies and temperatures (curves *2–5* and *6–8* in Fig. 2b). These data allow us to attribute the relaxation processes to the cation part of the crystal frame (sodium cations), since the anionic part consisting of MeO_6 and PO_4 polyhedra forms a rigid rhombohedral crystal frame $\{[Me_2(PO_4)_3]^{-3}\}_{3\infty}$ (*Me* = Sc or Cr [5, 6]). Therefore, the observed relaxation processes can be caused by the oscillations of low-mobility sodium cations (compensated sodium dipoles) in the *B* cavities of the crystal frame under the action of electric field and temperature (above 348 K).

At the next phase transitions, α' → β and β → γ, the relaxation processes are sharply accelerated and shift toward higher frequencies, which is shown by the corresponding curves in the ε(ω) and tanδ(ω) dependences (curves *6–8* in Figs. 2a and 2b). The occurrence of the fast relaxation processes can be caused by a sharp increase in the concentration of free and high-mobility sodium cations in the crystal frame of the sample due to the dipole disordering.

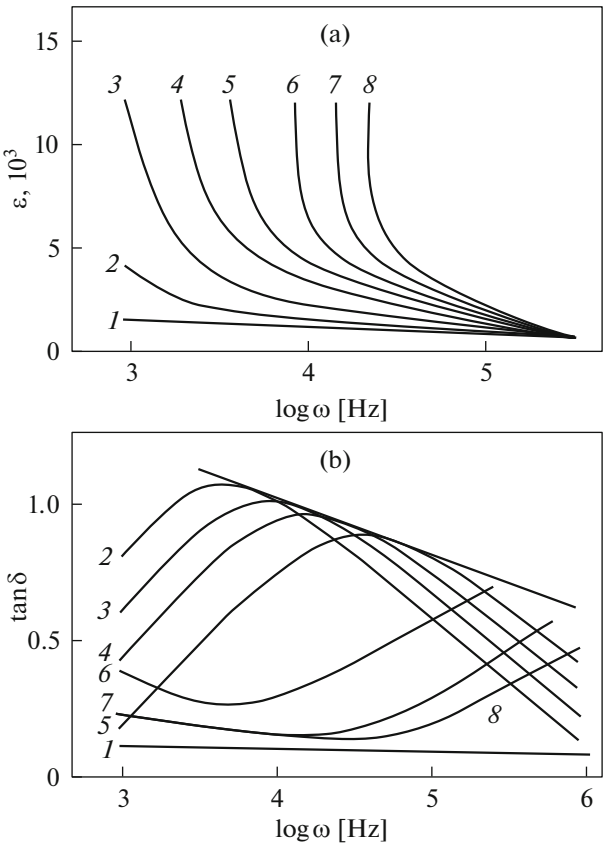

Fig. 2. Frequency dependences of (a) permittivity and (b) dissipation factor for the single-crystal $Na_3Cr_2(PO_4)_3$ sample. Curves *1–8* correspond to the measurements performed at temperatures of (*1*) 295, (*2*) 383, (*3*) 393, (*4*) 403, (*5*) 410, (*6*) 433, (*7*) 473, and (*8*) 483 K.

In studying the interaction between the electromagnetic field and a crystal, it is very useful to consider the sample under study as a two-pole consisting of circuit elements with the concentrated parameters. We built an equivalent circuit that corresponds best to the material under study (Fig. 3a). In this case, the α-$Na_3Cr_2(PO_4)_3$ crystal is replaced by circuit elements, i.e., capacitances C_1 and C_2 and resistance R_2. According to [7], the total conductivity of this equivalent circuit with the parameters C_1, R_2, and C_2 (Fig. 3a) is determined as

$$Y = \left(j\omega C_1 + \frac{1}{Z_2} \right), \qquad (2)$$

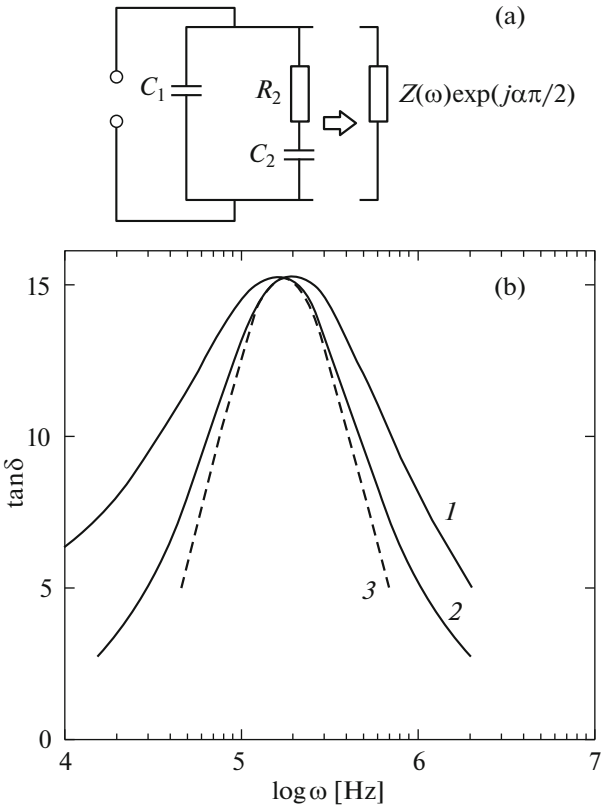

Fig. 3. (a) Equivalent circuit with the parameters $C_1 = 1.3 \times 10^{-7}$ F, $C_2 = 2.7 \times 10^{-6}$ F, and $R_2 = 5.78$ Ω corresponding to the dielectric α'-$Na_3Cr_2(PO_4)_3$ phase is changed for the circuit with the impedance $Z(\omega)\exp(j\pi\alpha/2)$ and C_1. (b) Curve *1* is the frequency dependence of the dissipation factor tanδ(ω) for the α-$Na_3Cr_2(PO_4)_3$ phase; curve *2* corresponds to the equivalent circuit with parameters C_1, R_2, and C_2; and curve *3* characterizes the Debye polarization relaxation.

where C_1 plays the role of a shunting capacitor and the complex impedance Z_2 of electric circuit R_2 and C_2 corresponds to the bulk resistance of the α-$Na_3Cr_2(PO_4)_3$ single crystal

$$Z_2 = R_2 + \frac{1}{j\omega C_2}. \quad (3)$$

To determine whether the equivalent circuit in Fig. 3a corresponds well to the single-crystal α'-$Na_3Cr_2(PO_4)_3$ sample, it is necessary to calculate the frequency dependence of this circuit using the expression [7]

$$\tan\delta = \frac{\omega\tau_2}{1 + \dfrac{C_1}{C_2(t + \omega^2\tau^2)}}, \quad (4)$$

where C_1 and C_2 are the capacitances of the first and second capacitors, respectively; τ_2 is the relaxation time equal to the product of resistance R_2 and capacitance C_2; and ω is the electromagnetic field frequency.

It can be seen from the plot in Fig. 3b that curve *2* with the maximum dissipation factor in the frequency dependence tanδ(ω) corresponding to the equivalent circuit with the parameters $C_1 = 1.3 \times 10^{-7}$ F, $C_2 = 2.7 \times 10^{-6}$ F, and $R_2 = 5.78$ Ω (Fig. 3a) is similar to experimental curve *1* built using the dielectric measurement data for the α'-$Na_3Cr_2(PO_4)_3$ sample (curves *1* and *2* in Fig. 3b).

On the other hand, the relaxation spectra in the frequency characteristic of α'-$Na_3Cr_2(PO_4)_3$ can be classified as Debye peaks, since the experimental characteristic of the sample (curve *1*) is similar to Debye curve *3* in Fig. 3b, which was built according to Debye formula (2) [8]

$$\tan\delta = \frac{\sigma}{\omega} + \frac{(\varepsilon_0 - \varepsilon_\infty)}{\varepsilon_0 + \varepsilon_\infty\omega^2\tau^2}, \quad (5)$$

where τ is the dipole relaxation time in the dielectric under the action of the external field; ε_0 and ε_∞ are the static and optical permittivities, respectively; and σ is the ionic conductivity.

The established equivalent circuit (Fig. 3a) allows us to conclude that the circuit portion R_2C_2 can correspond to the Debye dipole and the shunting capacitor C_1, to the friction during dipole rotation in the crystal.

However, the differences between the experimental (curve *1*) and calculated (curve *2*) frequency characteristics tanδ(ω) (Fig. 3b) evidence for the fact that the parameters of relaxation spectra for α'-$Na_3Cr_2(PO_4)_3$ are spread and the obtained dispersion data do not correspond to the hemisphere in the Cole–Cole diagram coordinates. The interrelation between the real (ε') and imaginary (ε'') permittivity parts for the α'-, β-, and γ-$Na_3Cr_2(PO_4)_3$ phases is presented in the form of the Cole–Cole diagram and shown in Fig. 4.

The Cole–Cole diagram for α'-$Na_3Cr_2(PO_4)_3$ (Fig. 4) has the form of a hemisphere with the center 0_1 located below the abscissa axis (curve *1*). For the superionic β- and γ-$Na_3Cr_2(PO_4)_3$ phases, the experimental points fit exactly hemispheres with the centers lying on the abscissa axis (see hemispheres *2* and *3* in Fig. 4).

To describe the dispersion of complex permittivity ε of the dielectrics with the spread spectra, it is reasonable to use the Cole–Cole empirical equation [8]

$$\varepsilon^x = \frac{\varepsilon_\infty + (\varepsilon_0 - \varepsilon_\infty)}{[1 - (j\omega\tau)^{1-\alpha}]}, \quad (6)$$

where α is the distribution coefficient characterizing the distribution of dipole relaxation times.

It can be seen from (6) that at $\alpha = 0$ the expression for ε exactly corresponds to the Debye dispersion of the permittivity.

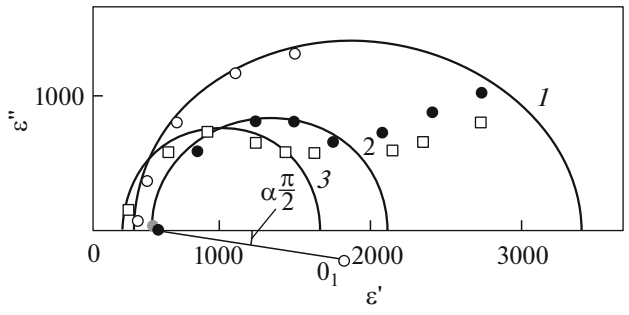

Fig. 4. Cole–Cole diagrams for different $Na_3Cr_2(PO_4)_3$ crystal phases: (*1*) semicircumference for the α' phase at 383 K, (*2*) semicircumference for the β phase at 433 K, and (*3*) semicircumference for the γ phase at 463 K.

The coefficients of distribution of the dipole relaxation times α for different phases of the $Na_3Cr_2(PO_4)_3$ sample were determined from the Cole–Cole diagrams presented in Fig. 4 and given in Table 2.

It can be seen from Table 2 that α'-$Na_3Cr_2(PO_4)_3$ is characterized by the distribution coefficient α = 0.062, which indicates the presence of several types of relaxators with the different relaxation times. At the phase transition to the β- and γ-$Na_3Cr_2(PO_4)_3$ phases, the distribution coefficients α are zero, which shows the presence of relaxators of the same type with the same relaxation time for all particles.

Equation (6) for α'-$Na_3Cr_2(PO_4)_3$ is more suitable for describing the permittivity dispersion. The equivalent circuit with the parameters $Z_2(\omega)\exp(j\pi\alpha/2)$ and C_1 for α'-$Na_3Cr_2(PO_4)_3$ shown in Fig. 3a correspond to the more general electric circuit (Fig. 3b) and characterizes the sample more exactly than the circuit with resistance R_2 and capacitance C_2, since the distribution coefficient α is taken into account.

In this case, $Z_2(\omega)$ is meant to be an impedance of the sample under study. Since in α'-$Na_3Cr_2(PO_4)_3$ we observe a set of the relaxation times, their values are difficult to determine. However, determination of the mean value of particle relaxation is quite possible, since we know the dissipation factor maxima for the frequency dependence tanδ(ω) of α'-$Na_3Cr_2(PO_4)_3$. Building the dependences $\omega_{max}(T)$, one can determine the activation energy E and average relaxation time τ at zero temperature for this phase. Then, the relaxation time τ can be determined according to [7] in the form

$$\tau = \frac{1}{2}\nu \exp(E/kT), \qquad (7)$$

where ν is the frequency of dipole self-oscillations, $\exp(E/kT)$ is the probability of overcoming the potential barrier with height E separating dipoles in their stable state by a dipole particle, and k is the Boltzmann constant.

The parameters of the relaxation polarization for α'-$Na_3Cr_2(PO_4)_3$ (Fig. 2) determined by the above-described methods are given in Table 2. The parameters of the relaxation polarization processes for the β and γ phases of this compound were determined by analyzing the frequency dependence of the dissipation factor.

Taking into account the established structural data for α-$Na_3Cr_2(PO_4)_3$ and results reported in [5, 6], as well as the frequency characteristics ε(ω) and tanδ(ω) presented in Fig. 2, we may conclude that the dipole ordering of sodium cations in α-$Na_3Cr_2(PO_4)_3$ is a system of coupled low-mobility dipoles in the *B* cavities of the crystal frame. Based on the specific features of population of the *A* and *B* cavities of the $Na_3Sc_2(PO_4)_3$ crystal frame by sodium cations [6, 9, 10], we may speak about the analogous character of population of the *B* planes of the $\{[Cr_2(PO_4)_3]^{P-}\}_{3\infty}$ crystal frame in the isostructural analog α-$Na_3Cr_2(PO_4)_3$ by sodium cations, which leads to the formation of statistical sodium dipoles.

In α-$Na_3Sc_2(PO_4)_3$ [6, 9, 10], the statistical sodium dipoles were formed by means of the nonuniform population of sodium cations in the *B* cavities of the crys-

Table 2. Parameters of the structure and relaxation polarization of the $Na_3Cr_2(PO_4)_3$ single crystal

$Na_3Cr_2(PO_4)_3$ parameters	Values			
Phase	α	α'	β	γ
Symmetry	$P2_1/n$	$P2_1/n$	$R3C$	$R3C$
Distribution coefficient α_p	–	0.062	0	0
ε_0	–	120	280	80
ε_ω	–	3200	1880	1600
Activation energy E, eV	–	0.393	0.262	0.213
Relaxation time τ, s	–	3.5×10^{-3}	1.3×10^{-5}	1.7×10^{-6}
Splitting of the Na_2 positions	2.17	2.21	–	20.26
	0.83; 1.33	0.84; 1.37	–	–

tal frame caused by splitting of Na_2 sodium positions into two unequal parts, which is equivalent to the formation of nonpolar sodium dipoles. Probably, it is the occurrence of such sodium dipoles that leads to the shift of the center of resulting positive charges (sodium compensating cations) relative to the center of the *B* cavity of the crystal frame. On the other hand, at the center of the *B* cavity, a center of resulting negative charges induced by the anion $\{[Sc_2(PO_4)_3]^{P-}\}_{3\infty}$ crystal frame should be focused.

Thus, we may draw a conclusion about separation of the centers of the positive and negative charges around the center of the *B* cavity in the crystal frame, which is equivalent to the formation of virtual polar sodium dipoles or statistical sodium dipoles in the crystal.

In the case of α- and α'-$Na_3Cr_2(PO_4)_3$, the dipoles are also meant to be polar sodium dipoles caused by the splitting of the Na_2 sodium positions in the *B* cavities of the crystal frame (the data on the Na_2 splitting were obtained in [5] and are given in Table 2). However, using the results of our study, we can make a conclusion about the existence of compensated statistical sodium dipoles. This is consistent with the fact of doubling the unit cell volume in α-$Na_3Cr_2(PO_4)_3$ established by X-ray investigations. This is indicated by the absence of a SHG signal and the stability of dielectric parameters α and tanδ at low temperatures over the entire frequency range.

According to the structural data from [5], the α'-$Na_3Cr_2(PO_4)_3$ crystal frame is monoclinically distorted. However, the data on the conductive and dielectric properties suggest that the distortion of the α'-phase crystal frame is pronounced weaker than in α-$Na_3Cr_2(PO_4)_3$, which can be attributed to the partial elimination of the crystal frame distortion and the occurrence of charges with the higher mobility. These changes can explain the observed heat relaxation polarization in α'-$Na_3Cr_2(PO_4)_3$ (Fig. 2).

The relaxation polarization process caused by the motion of sodium cations in cavities of the rhombohedral $\{Cr_2(PO_4)_3]^3\}_{3\infty}$ crystal frame is equivalent to throwing the compensated statistical sodium dipoles over the potential barrier $E = 0.92$ eV for the average time $\tau = 3.5 \times 10^{-3}$ s.

According to the representation of such an interaction of sodium dipoles with the ac electric field in α'-$Na_3Cr_2(PO_4)_3$, the equivalent circuit of this sample shown in Fig. 3a is quite acceptable, since the shunting capacitor C_1 reflects the interaction of relaxing particles.

3.4. On Potential Barrier and Relaxator Models for α- and α'-$Na_3Cr_2(PO_4)_3$

For the systems where the relaxation on the microscopic scale is described by Eq. (4), we can use a deep potential well model with two equilibrium positions or Flerikh relaxator (Fig. 5a). Based on this model and the model for the dielectric α'-$Na_3Sc_2(PO_4)_3$ phase proposed in [9, 10], as well as on the data on the conductive dielectric properties and structural parameters of the α-$Na_3Cr_2(PO_4)_3$ phase, we can propose a model of two-minimum potential relief along the conductivity channel (Fig. 5a). It should be noted that the depth of potential relief (energy characteristic) in the model depends on the degree of structural distortions of the crystal frame.

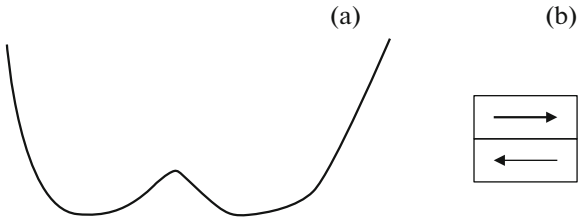

Fig. 5. Schematic image of the potential barrier and compensated sodium dipole for α-$Na_3Cr_2(PO_4)_3$. (a) Image of the potential well with two equilibrium positions and (b) image of the compensated statistic sodium dipole.

In α'-$Na_3Cr_2(PO_4)_3$, the depth of the potential relief will be lower than for α-$Na_3Cr_2(PO_4)_3$ and the relaxator at the relaxation polarization can be a compensated statistical sodium dipole. Figure 5b schematically shows a sodium dipole formed from two oppositely directed statistical sodium dipoles due to the doubling of the crystal unit cell volume.

3.5. On the Polarization Processes in the β- and γ-$Na_3Cr_2(PO_4)_3$ Phases

The transition to β-$Na_3Cr_2(PO_4)_3$ is accompanied by the partial destruction of statistical sodium dipoles, which is indicated by the high ionic conductivity, jump in the temperature dependence (Fig. 1), and established dielectric (Fig. 2) and structural parameters.

Note that β-$Na_3Cr_2(PO_4)$ has a quasi-rhombohedral structure analogous to the β-$Na_3Sc_2(PO_4)_3$ phase, which unambiguously follows from the phase diagram of the $Na_3Sc_2(PO_4)_3$–$Na_3Cr_2(PO_4)_3$ system [11]. All the results agree well with the fact that the relaxators are only free sodium ions (the distribution coefficient α of the β phase is zero). The dissipation factor maxima for this phase are shifted toward higher frequencies and pass beyond the frequency range of our investigations on the single-crystal samples. The observed tales of curves *7* and *8* in the frequency dependence tanδ(ω) and curves *6* and *7* (Fig. 2b) evidence for the fact that the relaxation polarization process shifts toward higher frequencies. It is quite reasonable to attribute these polarization processes to the fast oscillations of sodium atoms in the crystal frame of the β phase under the action of the external electric field. In

addition, the permittivities of β-$Na_3Cr_2(PO_4)_3$ at zero and infinite frequencies, which reflect the interrelation of ε' and ε'' via the Cole–Cole diagram, are characterized by the smaller circumference (curve *2* in Fig. 4) than in the case of α'-$Na_3Cr_2(PO_4)_3$ phase.

The above-mentioned features of the dielectric properties of β-$Na_3Cr_2(PO_4)_3$ are even more pronounced at the transition to the rhombohedral γ-$Na_3Cr_2(PO_4)_3$ phase ($3\bar{R}C$), which can be related to the maximum increase in the symmetry of the rhombohedral crystal frame, which leads to a decrease in the potential barrier and complete disordering of compensated statistical sodium dipoles. The high mobility and uniform distribution of sodium ions over the *A* and *B* cavities of the rhombohedral crystal frame provides the conditions for the occurrence of rapid polarization processes under the action of an rf electric field.

3.6. On the Dipole Ordering Model in the α and α' Phases and Ionic Conductivity in the β and γ Phases of $Na_3Cr_2(PO_4)_3$

The processes of structural disordering at the phase transitions α → β and β → γ occur in also $Na_3Sc_2(PO_4)_3$ and lead to the variations in the properties [1, 9] similar to those in sodium chromium phosphate. However, the dipole ordering character in the monoclinic α-$Na_3Sc_2(PO_4)_3$ phase is related to statistical sodium dipoles [9, 10]. The features of the structure and properties of $Na_3Cr_2(PO_4)_3$ can be judged by the results reported in [5, 9–11].

As was shown in [9, 10], the $Na_3Sc_2(PO_4)_3$ crystal structure is based on the skeletal $\{[Sc_2(PO_4)_3]^{3-}\}_3$ crystal frame with three-dimensional channels. These channels are formed by joining the *A* and *B* cavities by corrugated hexagonal rings. The *A* cavities are smaller than the *B* cavities. In α-$Na_3Sc_2(PO_4)_3$, sodium cations are ordered in the *B* cavities in statistical sodium dipoles formed due to the monoclinic distortions of the frame. At the transition to the high-temperature β and γ phases, the structural distortions are eliminated and sodium atoms can be statistically distributed in both the *A* and *B* cavities.

Thus, we may conclude that at the monoclinic distortions of the $\{[Me_2(PO_4)_3]^3\}_{3\infty}$ (*Me* is a trivalent metal) crystal frame, the NASICON structural-type compounds form statistical dipoles of two types: uncompensated, as in α-$Na_3Sc_2(PO_4)_3$ [9], and compensated, as in α-$Na_3Cr_2(PO_4)_3$. However, due to the elasticity of such a crystal frame, which manifests itself at the phase transitions α → β and β → γ, the structural distortions are completely eliminated at the simultaneous destruction of statistical dipoles. Under the action of electromagnetic fields, the β- and γ-$Na_3Cr_2(PO_4)_3$ phases are characterized by the occurrence of fast relaxation processes, which can be described by the Debye model.

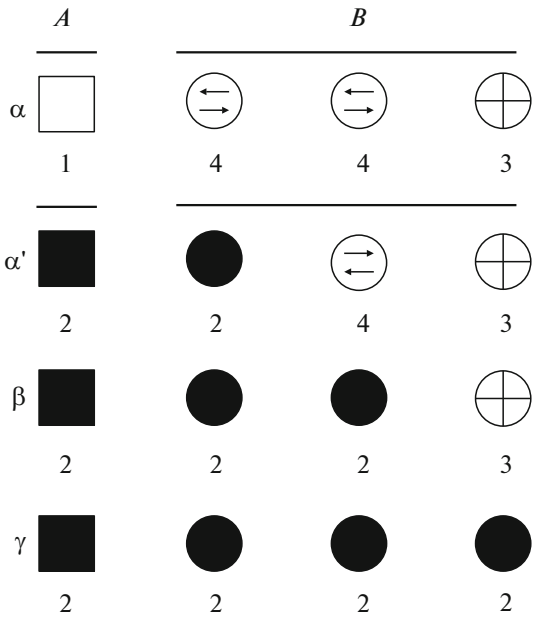

Fig. 6. Crystallochemical model explaining the conventional distribution of sodium atoms over the *A* and *B* cavities in the crystal frame of the α-, α'-, β-, and γ-$Na_3Cr_2(PO_4)_3$ phases. (*1*) Vacant *A* cavity, (*2*) statistical population of positions in the *A* and *B* cavities of the crystal frame by sodium cations. (*3*) Population of sodium cations with the ordering in the *B* cavities of the crystal frame. (*4*) Compensated statistical sodium dipole in the *B* cavities of the crystal frame.

According to the data from [5, 6] and in view of the generality of the structures and properties of sodium scandium and chromium phosphates, the distribution of sodium atoms over the *A* and *B* cavities of the crystal frame for the α-, α'-, β-, and γ-$Na_3Cr_2(PO_4)_3$ phases can be schematically presented as in Fig. 6. In this case, the *A* cavities can be vacant or statistically occupied by sodium atoms and the *B* cavities can be statistically occupied with the ordering or in the form of statistical sodium dipoles.

The vacant *A* cavities are shown in Fig. 6 by bright square *1* and the ordered states and compensated statistical sodium dipoles in the α- and α'-$Na_3Sc_2(PO_4)_3$ crystal frames are denoted as *3* and *4*, respectively (Fig. 6). The statistical population of the *A* and *B* cavities of the crystal frame in α'-, β-, and γ-$Na_3Cr_2(PO_4)_3$ phases by sodium cations is denoted as *2* in Fig. 6.

It is worth noting that the α-$Na_3Sc_2(PO_4)_3$ crystal is polar and its surface contains domains; therefore, it was classified as a ferroelectric [12]. It is quite reasonable to assume that a part of *B* cavities in α-$Na_3Cr_2(PO_4)_3$ is occupied by compensated statistical sodium dipoles (*4* in Fig. 6).

According to this model, α-$Na_3Cr_2(PO_4)_3$ is characterized by both ordered and dipole-ordered states in the *B* cavity of the crystal frame (*3* and *4* in Fig. 6). In this case, the *A* cavities are completely vacant.

At the next phase transitions α' → β and β → γ in the $Na_3Cr_2(PO_4)_3$ crystal, the events of a sequential crystal symmetry increase occur, which lead to the destruction of the dipole-ordered states and more uniform statistical distribution of sodium cations over the *A* and *B* cavities of the crystal frame, as is shown in Fig. 6 for β- and γ-$Na_3Cr_2(PO_4)_3$.

4. CONCLUSIONS

Based on the presented experimental results, we can make the following conclusions:

(i) It was proved that the α-$Na_3Cr_2(PO_4)_3$ crystal structure is characterized by the superstructural antiferroelectric ordering. At the phase transitions α → α', α' → β, and β → γ in the $Na_3Cr_2(PO_4)_3$ crystal, the events of a sequential crystal symmetry increase occur. The α'-$Na_3Cr_2(PO_4)_3$ crystal is a dielectric, although its conductivity is higher than that of α-$Na_3Cr_2(PO_4)_3$ due to the partial elimination of the monoclinic distortion of the crystal frame. A noticeable increase in the conductivity at the phase transition α' → β, yet an insignificant decrease in the activation energy allow us to consider β-$Na_3Cr_2(PO_4)_3$ as an almost superionic phase.

A noticeable increase in the conductivity and the corresponding activation energy drop at the phase transition β → γ allow us to conclude that γ-$Na_3Cr_2(PO_4)_3$ is a superionic conductor.

(ii) It was demonstrated that the α-$Na_3Cr_2(PO)_3$ structure facilitates the formation of low-mobility compensated statistical sodium dipoles weakly interacting with the external electric field. It was established that the relaxation polarization in the dielectric α'-$Na_3Cr_2(PO)_3$ phase has a Debye character and the relaxators are compensated sodium dipoles. The β and γ phases are characterized by the fast relaxation processes caused by the presence of mobile sodium cations in the *A* and *B* cavities of the crystal frame.

The crystallochemical model was proposed, which explains the phenomena of dipole ordering and ionic conductivity in $Na_3Cr_2(PO_4)_3$.

REFERENCES

1. A. S. Nogay, Young Huh, and K. N. Yugay, Phys. Solid State **47**, 1076 (2005).
2. A. Nogai, V. B. Kalinin, S. Yu. Stefanovich, Yu. N. Venevtsev, and V. V. Gagulin, Zh. Neorg. Khim. **33**, 747 (1988).
3. L. Vijayan, R. Cheruku, G. Govindaraj, and S. Rajagopan, Mater. Chem. Phys. **130**, 862 (2011).
4. L. B. Ellis and F. Linda, Curr. Opin. Solid State Mater. Sci. **16**, 168 (2012).
5. F. d'Yvoire, M. Pintard-Serépel, E. Bretey, and M. de la Rochér, Solid State Ionics, Nos. 9–10, 851 (1983).
6. V. B. Kalinin, S. Yu. Stefanovich, and A. C. Nogai, Neorg. Mater. **22**, 107 (1986).
7. A. R. Hippel, *Dielectrics and Waves* (Wiley, New York, 1954).
8. Yu. M. Poplavko, *Physics of Insulators* (Vyssh. Shkola, Kiev, 1980) [in Russian].
9. V. A. Efremov and V. B. Kalinin, Sov. Phys. Crystallogr. **23**, 393 (1978).
10. V. B. Kalinin, B. I. Lazoryak, and S. Yu. Stefanovich, Sov. Phys. Crystallogr. **28**, 154 (1983).
11. V. B. Kalinin, S. Yu. Stefanovich, R. R. Shifrina, and Yu. N. Venevtsev, Zh. Neorg. Khim. **31**, 181 (1986).
12. S. A. Okonenko, S. Yu. Stefanovich, V. B. Kalinin, and Yu. N. Venevtsev, Sov. Phys. Solid State **20**, 1647 (1978).

Translated by E. Bondareva